

Exploring the Sgr–Milky-Way-disc interaction using high resolution N -body simulations

Morgan Bennett^{1*}, Jo Bovy¹, & Jason A. S. Hunt²

¹ Department of Astronomy and Astrophysics, University of Toronto, 50 St. George Street, Toronto, Ontario, M5S 3H4, Canada

² Center for Computational Astrophysics, Flatiron Institute, 162 5th Av., New York City, NY 10010, USA

ABSTRACT

The ongoing merger of the Sagittarius (Sgr) dwarf galaxy with the Milky Way is believed to strongly affect the dynamics of the Milky Way’s disc. We present a suite of 13 N -body simulations, with 500 million to 1 billion particles, modelling the interaction between the Sagittarius dwarf galaxy (Sgr) and the Galactic disc. To quantify the perturbation to the disc’s structure and dynamics in the simulation, we compute the number count asymmetry and the mean vertical velocity in a solar-neighbourhood-like volume. We find that overall the trends in the simulations match those seen in a simple one-dimensional model of the interaction. We explore the effects of changing the mass model of Sgr, the orbital kinematics of Sgr, and the mass of the Milky Way halo. We find that none of the simulations match the observations of the vertical perturbation using *Gaia* Data Release 2. In the simulation which is the most similar, we find that the final mass of Sgr far exceeds the observed mass of the Sgr progenitor, the asymmetry wavelength is too large, and the shape of the asymmetry doesn’t match past $z \approx 0.7$ kpc. We therefore conclude that our simulations support the conclusion that Sgr alone could not have caused the observed perturbation to the solar neighbourhood.

Key words: Galaxy: disc — Galaxy: kinematics and dynamics — Galaxy: structure — Galaxy: evolution — solar neighbourhood — Galaxy: formation

1 INTRODUCTION

The Milky Way has been the ideal location to study galactic dynamics because our position inside the Galactic Disc gives us the perfect view of stars’ motions. With surveys like *Gaia* (Gaia Collaboration et al. 2018a) we have an unprecedented amount of data on the dynamics of stars in the solar neighbourhood. However, observing from inside the disc can also complicate matters. It’s difficult to get a holistic view of what’s going on when you’re moving inside the Galactic Disc. In addition to this, stars are obscured and reddened by dust in the sight-line. For this reason, it is useful to have galactic simulations to supplement our knowledge and test theories and models. Simulations have been an important tool for investigating our Milky Way for a few decades now (Kuijken & Dubinski 1995; Ibata & Lewis 1998; Fux 1999). While analytical calculations have been extraordinarily useful, it has been simulations which have been most able to reproduce the properties of observed galaxies (e.g. Navarro et al. 1996; Tormen et al. 1997; Jenkins et al. 1998, 2001). This is because there are so many things affecting the dynamics of the Milky Way, that it’s impossible to capture them all in one model and typically we focus on the dominant effect or make assumptions of symmetry or equilibrium. N -body simulations do not require these simplifications.

The existence of a vertical perturbation to the Galactic disc has

been an area of study for almost a decade (Widrow et al. 2012). Evidence shows that the Galactic Disc has recently undergone some fairly large perturbations on the order of $\sim 10\%$ (Antoja et al. 2018; Kawata et al. 2018; Bennett & Bovy 2019). To quantify the perturbation, people have examined the number count asymmetry, trends in the mean vertical velocity, and 2-dimensional phase-space (Yanny & Gardner 2013; Antoja et al. 2018; Bennett & Bovy 2019; Carrillo et al. 2019). Despite this, the origin of the perturbation remains unknown. One consideration is the bar buckling as a method of producing the perturbations seen in the solar neighbourhood. Khoperskov et al. (2019) did a small scale simulation ($\sim 10^8$ particles) and were only able to reproduce a qualitative match to the vertical phase-space perturbation. The most commonly discussed cause of the vertical perturbation is the recent passage of the Sgr dwarf galaxy. One of the most prominent investigations into the perturbation in the Milky Way disc predates the discovery of the phase-space spiral. Laporte et al. (2018) explores how the force from the Sagittarius Dwarf Galaxy (Sgr) and the Large Magellanic Clouds (LMC) affects the equilibrium of the Milky Way. They look beyond just the one dimensional vertical perturbation and also consider the effect as a function of radius and find that Sgr causes corrugation and flaring of the disc. The effects due to Sgr for that simulation are then further analysed in Laporte et al. (2019) where they compared it to the observed phase-space spiral. They find that there is a qualitative match, but are not able to reproduce the perturbation wavelength with their simulations. Further, while they

* E-mail: bennett@astro.utoronto.ca

consider 4 mass models for Sgr in the first paper, the second paper only focuses on one orbit for one of the lighter Sgr models.

While there have been many simulations which use Sgr-like conditions to investigate the effect on the Milky Way, it has been difficult to quantify how well they are able to reproduce observations. With so many simulations out there, it is hard to compare the results in the different simulations because of the varying methods behind them all. Finally, it has also been difficult to explore how the properties of Sgr affect the observed perturbations using simulations, because it requires a large number of particles which is computationally expensive. By utilising a GPU N -body tree-code, we are able to overcome this and quickly run simulations with 500 million to 1 billion particles (e.g. Hunt et al. 2021). Vasiliev & Belokurov (2020) perform an in depth analysis of the kinematics of Sgr including finding the mass of the progenitor, $\sim (4 \pm 1) \times 10^8 M_{\odot}$, where approximately 25% comes from the stellar component. They also investigate how the initial structure of Sgr relates to the observed progenitor today and are able to reproduce the cigar-like shape using spherical models. The Sgr mass models used in our analysis are all based on the models studied in Vasiliev & Belokurov (2020).

In Section 2, we discuss the techniques we use to initialise the initial conditions for our 3-dimensional N -body simulations. We also discuss how we choose where to place Sgr in our Milky Way for the simulations and include a brief discussion about the properties of our equilibrium simulations before placing Sgr. In Section 3, we discuss the properties of solar neighbourhood-like volumes in each of our simulations. The Section is broken down into three further sections where we look at the effects of changing (i) the mass of Sgr, (ii) Sgr's orbit, and (iii) the mass of the Milky Way halo. Finally, in Section 4 we discuss our findings, their implications, and how to move forward.

2 NUMERICAL METHODS

To create the initial conditions for our N -body simulation, we use GALIC: Galaxy initial conditions construction¹ (Yurin & Springel 2014) to setup the Milky Way and, separately, Sgr. We then simulate the evolution of the Milky-Way–Sgr system using Bonsai² (Bédorf et al. 2012). In this section, we discuss all of the ingredients of our numerical methods in detail.

2.1 Model for the Milky Way

For the purposes of our investigation, we choose to look at three different Milky Way models. The models are derived from the galpy potential MWPotential2014, but with heavier halos and match the potentials in Bennett & Bovy (2021, hereafter BB21): MWP14-1, MWP14-2, and MWP14-3. In BB21, we showed that the heavier Milky Way potentials were the only two which led to realistic looking asymmetries. However, for the sake of completeness, we also run simulations for the MWP14-1 model. All three potential models have the same disc and bulge as MWPotential2014, but while MWP14-1 also has the same halo as MWPotential2014, MWP14-2 and MWP14-3's halos are 1.5 and 2 times heavier than the MWPotential2014 one, respectively. We use MWP14-2 to investigate how a changing Sgr mass affects the perturbation as well as how changing the dynamics of Sgr and use approximately 1 billion particles in

Parameters	MWP14-1	MWP14-2	MWP14-3
CC	9.0139	10.4295	11.6131
V200	142.0	165.4	184.7
LAMBDA	0.0526	0.0468	0.0441
MD	0.1002	0.0636	0.0458
MB	0.00676	0.00428	0.00307
JD	0.1002	0.0636	0.0458
Disk Height	0.0933	0.0933	0.0933
Bulge Size	0.0203	0.01936	0.0188
Halo Stretch	1.0	1.0	1.0
Bulge Stretch	1.0	1.0	1.0
N_{HALO}	40,000,000	40,000,000	40,000,000
N_{DISK}	50,000,000	50,000,000	50,000,000
N_{BULGE}	10,000,000	10,000,000	10,000,000
Halo Velocity Structure	0	0	0
Disk Velocity Structure	3	3	3
Bulge Velocity Structure	0	0	0
Disk Dispersion R over Z ratio	1.874	1.874	1.874
Disk Streaming Velocity	0.985	0.985	0.985

Table 1. GalIC parameters to generate the initial conditions for the three different Milky Way models.

our MWP14-2 simulations and approximately 500 Million in our MWP14-1 and MWP14-3 simulations. MWP14-1 and MWP14-3 are only used to compare how a changing halo mass affects the perturbation. For thoroughness, we do look at the fastest, median, and slowest orbits for these two additional initial conditions. For the purpose of this section, we will thoroughly explain how we obtained the initial conditions for MWP14-2 since the method was the same for all Milky Way equilibrium conditions and then include the parameters for all three in Table 1

When considering the parameters of the halo, we need to take into account that MWPotential2014 uses an NFW halo, but GALIC assumes a Hernquist profile for the halo, so we need to convert from one to the other. Calculating the GALIC parameters is not entirely straight forward since GALIC uses a definition where $r_{200} = v_{200}$ for the entire Milky Way. Furthermore, r_{200} is used to calculate the total mass of the galaxy and r_{200} and the concentration c , are used to calculate the scale radius of the halo. This means that r_{200} is both a property of the entire galaxy as well as a property of the halo. So we need to artificially increase the concentration parameter such that a_h matches the scale radius of the halo in MWPotential2014. We start by using the true r_{200} and concentration, c , of the NFW halo in MWPotential2014 to calculate the desired Hernquist scale radius using:

$$a_h = \frac{r_{200}}{c} \sqrt{2 \left[\ln(1+c) - \frac{c}{1+c} \right]} \quad (1)$$

This gives us a Hernquist scale radius of $a_h = 27.68$ kpc. However, the r_{200} of the halo is *not* the same as the r_{200} parameter in GALIC. Therefore, we use the same equation above along with the newly calculated scale radius of $a_h = 27.68$ as well as the r_{200} which corresponds to a mass of the entire galaxy to calculate the corresponding concentration.

The next parameter we calculate is the disc spin parameter, λ :

$$\lambda = \frac{J_d}{m_d G^{1/2} M_{200}^{3/2} r_{200}^{1/2}} \quad (2)$$

where J_d is the disc angular momentum, m_d is the disc mass frac-

¹ <https://wwwmpa.mpa-garching.mpg.de/~volker/galic/>

² <https://github.com/treecode/Bonsai>

tion, and

$$f_c = \frac{c \left(1 - \frac{1}{(1+c)^2} - \frac{2 \ln(1+c)}{(1+c)} \right)}{2(\ln(1+c) - \frac{c}{(1+c)})^2} \quad (3)$$

(Springel & White 1999). For MWP14-2, the spin parameter works out to be approximately 0.047.

We find the disc and bulge mass fraction simply by calculating $M_d(R = r_{200}, z = r_{200})$ and $M_b(r = r_{200})$ and calculate for MWP14-2 that $m_d = 0.0636$ and $m_b = 0.00428$. Not to be confused with the disc angular momentum, the ‘JD’ parameter in GalIC is the disc spin fraction, and is equal to the mass spin fraction (assuming conservation of momentum of the material that forms the disc).

In GalIC you can set a starting point for the disc scale height and the initial guess for the scale radius of the disc is determined by λ , c and r_{200} . The final value for both the scale height and radius is ultimately determined iteratively using the disc momentum. The disc scale height is given in units of disc scale length, so we use the ratio of the disc scale height b and scale length a in MWPotential2014 to estimate this value to be 0.0933. Ultimately, GalIC settles on values of $H = 3.41$ kpc and $z_h = 0.318$ kpc.

The scale radius of the bulge, a_b , is given in units of the halo scale length, and we use a value of $a_b = 0.01936$. For both the bulge and the halo, we choose to have a spherically symmetric and isotropic velocity structure.

For the disc velocity structure, we choose an axisymmetric disc, described by a distribution function of the form $f(E, Lz, I_3)$ which requires $\langle v_z^2 \rangle / \langle v_R^2 \rangle$, and the net rotation specified. Since these parameters are not considered in MWP14-2 which is a static potential, we use the *Gaia* DR2 data in the solar neighbourhood to estimate both. For the velocity dispersion ratio, we find a value of approximately $\langle v_R^2 \rangle / \langle v_z^2 \rangle = 1.874$. This is approximately consistent with Mackereth et al. (2019) who found a value of $\sigma_R / \sigma_z = 1.56 \pm 0.10$. The net rotation is given by the disc streaming parameter, k , which is calculated using:

$$k^2 = \frac{\langle v_\phi \rangle^2}{\langle v_\phi^2 \rangle - \sigma_R^2} \quad (4)$$

Again using *Gaia* DR2, we find $k = 0.985$ in the solar neighbourhood. For the different components, we use 5×10^8 particles in the disc, 10^8 in the bulge, 4×10^8 in the halo.

Due to computational constraints, instead of running one initial condition with 10^9 particles, we ran 10 (or 5 in the case of MWP14-1 and MWP14-3) initial conditions with 10^8 particles using random seeds 1000 through 10000. While each of the ten snapshots is in equilibrium, they are not necessarily in equilibrium with each other. This is not a concern since as we describe in Section 2.3, we run all conditions together for 3 Gyr before adding in Sgr.

2.2 Models for Sgr

The next step is choosing the models for the Sgr-like satellite in our simulation. We choose to look at the Sgr 1, Sgr 2, and Sgr 3 models from BB21 which are the three heaviest of the five considered. These models are derived from the Sgr parameters in Vasiliev & Belokurov (2020). Though they were ruled out in BB21, we choose the heaviest models because we wanted to generate the largest signal possible in our N -body simulation to overcome the uncertainties which come with having a small number of particles in the solar neighbourhood. The three Sgr mass models have halo masses of $M_{\text{sgr},h} = (50, 10, 5) \times 10^9 M_\odot$ and stellar masses

of $M_{\text{sgr},*} = (1, 0.2, 0.1) \times 10^9 M_\odot$. Both components are given as Hernquist potentials with scale radii of $a_{\text{sgr},h} = (6.7, 3.0, 2.1)$ kpc and $a_{\text{sgr},*} = (1.45, 0.65, 0.46)$ kpc. These two-component spherical models are consistent with the findings of Vasiliev & Belokurov (2020).

Like with the Milky Way, we also use GalIC to create the initial conditions for Sgr. By setting $M_{200} = M_{\text{sgr},h} + M_{\text{sgr},*}$, GalIC also sets V_{200} and R_{200} for the entire system. To make sure that the halo scale radius in GalIC matches the values above, we have to choose a concentration using Equation (1), therefore we set $c_{\text{sgr},h} = 17.96, 25.24, 29.15$. Our final choice when initializing Sgr with GalIC is the number of particles in each of the two components. This choice is fairly arbitrary, so we choose a number of particles in the Sgr dark matter halo such that their mass approximately matches the mass of the halo particles in our Milky Way, $m_{\text{mw},h} \approx 2451 M_\odot$. For the stellar particles in Sgr, we choose a number of particles such that they will have a similar mass to the particles in the Milky Way disc, $m_{\text{mw},d} = 133.8 M_\odot$. So this means that the halo has $N_{\text{sgr},h} = (20.4, 4.08, 2.04) \times 10^6$ and the stellar component has $N_{\text{sgr},*} = (7.5, 1.5, 0.75) \times 10^6$. Once we have generated the particles for Sgr, we have to decide where to place them relative to the centre of the Milky Way such that they end up near Sgr’s location today.

2.3 Simulations

The simulations are evolved using a gravitational N -body GPU tree code integrator *Bonsai*. There are five parameters which need to be specified for a simulation using *Bonsai*. For the opening angle we used a value of 0.4 which is typical, if not smaller than other simulations in the field (Laporte et al. 2018; Khoperskov et al. 2019). With *Bonsai*, you can specify the frequency with which you want to rebuild the tree which computes the forces, we update the tree at each step. *Bonsai* requires a constant integration time-step, for all simulations discussed in this paper we use 9.778145 kyr. For the simulations where we vary the mass of Sgr, the output time-step was every 4000 steps, but for the kinematics of Sgr simulations as well as varying the MW halo mass, we chose to output snapshots every 1000 steps. Finally, we use a softening parameter of 50 pc, which is on the order typically used for these types of simulations (Laporte et al. 2018; Vasiliev & Belokurov 2020). The entire suite of simulations took approximately 5 GPU years to run on Nvidia Tesla 32 GB V100 GPUs.

We ran the initial conditions of the Milky Way for 3 Gyr or more before adding Sgr to ensure the disc was in equilibrium as well as to get a better measure of the intrinsic uncertainty in the perturbation to the distribution function. Ideally, the perturbation function would be completely symmetric for our ‘equilibrium’ case, but due to the discrete nature of anybody simulations and intrinsic Poisson error, that is not the case. So when we measure the asymmetry in the perturbed simulation we have a baseline to compare against.

2.4 Validation

Before looking at the perturbed Milky Way, we first look at the equilibrium case to see how well we can trust any asymmetry seen in our perturbed simulation.

The first thing we check is that the properties of our disc are reasonable compared to that of the Milky Way. We examined eight solar neighbourhood-like volumes around the equilibrium Milky Way simulation spaced $\pi/4$ radians apart and starting at $\phi = 0$.

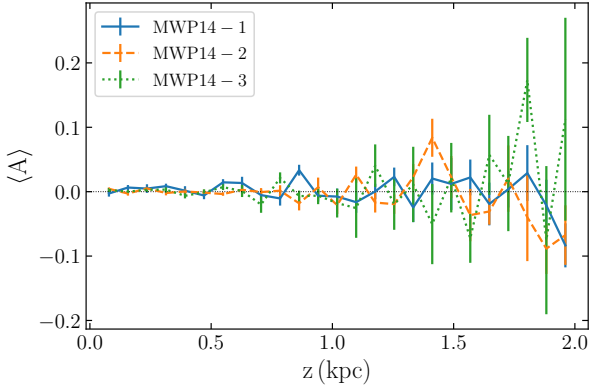


Figure 1. Mean asymmetry at 8 different solar neighbourhood like areas in the simulation which are at a radius of 8.1 kpc and spaced every 45 degrees around the circle starting at $\phi = 0$. The three lines represent the three different equilibrium simulations done for MWP14-1 (blue solid), MWP14-2 (orange dashed), and MWP14-3 (green dotted). This asymmetry for the unperturbed disc provides a baseline for comparison when considering the significance of the signal in our perturbed simulations.

They were all at a radius of 8.1 kpc from the centre of mass of the disc and bulge. The true mid-plane density has been measured to be approximately $\rho_0 = 0.1$ (Holmberg & Flynn 2000; Widmark & Monari 2019). The average mid-plane density of MWP14-1 is $(0.062 \pm 0.002) M_\odot \text{pc}^{-3}$ which is significantly lower than the mid-plane density in the Milky Way, which we will have to account for in our analysis. For MWP14-2, we found an average mid-plane density of $(0.116 \pm 0.006) M_\odot \text{pc}^{-3}$. For MWP14-3, the average mid-plane density fell at $(0.12 \pm 0.01) M_\odot \text{pc}^{-3}$. The average mid-plane density is high compared to true mid-plane density of the Milky Way, but the density is also affected by the introduction of Sgr, and therefore an exact match at this stage is not required. Next, we looked at the velocity dispersion of the simulated Milky Way discs and found that their mean velocity dispersion at the solar neighbourhood was $22.4 \pm 0.12 \text{ km s}^{-1}$, $22.8 \pm 0.3 \text{ km s}^{-1}$, and $22.3 \pm 0.4 \text{ km s}^{-1}$ for MWP14-1, MWP14-2, and MWP14-3 respectively. This is also similar to the true values of the Milky Way, which is approximately 20.5 km s^{-1} (Gaia Collaboration et al. 2018b; Bennett & Bovy 2021).

Second, we check that the Milky Way reaches an equilibrium before we add the satellite. To do this, we check the rotation curve of the galaxy at several different snapshots in the simulation. At first, the potential is smooth and well defined. After some time, a bar forms and we need to wait until the disc has reached equilibrium again before adding our satellite.

Finally, we check the density asymmetry as a function of height at our last time at several different Solar Neighbourhood-like locations throughout the Milky Way. We measure the asymmetry at the previously defined 8 different equally spaced locations in the Milky Way. Figure 1 shows the mean asymmetry as well as the error in the mean using those eight locations spaced equidistant around the circle at $R = 8.1$ kpc. For all three Milky Ways, the uncertainty as well as the asymmetry appear to grow at approximately equal rates. The figure clearly shows that within 1.3 kpc of the mid-plane, the asymmetry for MWP14-2 and MWP14-3 is within uncertainty of zero for both equilibrium Milky Ways. However, further out we see that the asymmetry grows faster than the uncertainty. The asymmetry of MWP14-1 actually stays within uncertainty of zero except for one small deviation at ~ 0.85 kpc at all heights. When looking

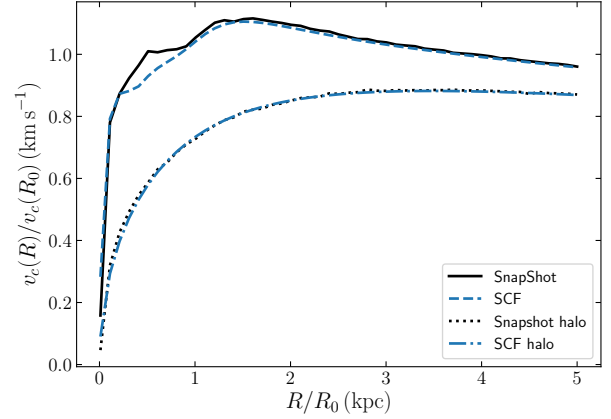


Figure 2. Rotation curve for the full three component galpy snapshot potential (black solid) as well as the SCF basis expansion potential (Blue dashed). Also plotted is the rotation curve for just the halo component of the snapshot potential (black dotted) and the SCF potential (blue dash-dot). While the three component potential is quite different within 8 kpc, they agree well further out and are fully consistent at all length scales for the halo.

at our perturbed simulations, it is important to keep in mind the heights at which we can trust our results.

2.5 Placing Sgr

To figure out where to place the satellite in our simulation such that it most resembles the Sgr satellite, we have to integrate Sgr’s present-day position backwards in the potential of our equilibrium simulation. There are several different methods for calculating the potential for the simulations. The first is the exact calculation. However, this can be computationally expensive and not feasible. For that reason, we decide to approximate the potential using the self-consistent field (SCF) basis function expansion described in Hernquist & Ostriker (1992). We use the galpy Python package³ to calculate the SCF expansion coefficients and initialise the potential using the expansion orders of $N_h = L_h = 5$ for the halo, $N_d = L_d = 15$ for the disc, and $N_b = L_b = 3$ for the bulge. The order of the expansion reflects the complexity of that component. The SCF expansion also requires that we define scale radii for each component. We use the Hernquist radius of the halo, the disk height, and the bulge size defined in Section 2.1 for the halo, disc and bulge respectively. Since the coefficients are additive, we calculate the coefficient on subsets of the particles for each component before adding them together to calculate the approximate potential expansion.

To ensure that the approximated potential behaves similarly to the actual potential of the particles, we test several different properties. The first thing we check is that the rotation curve calculated using each particle’s position and mass using direct summation matches the rotation curve of our SCF expansion. We calculate the direct-summation result using galpy’s SnapshotRZ which creates an axisymmetrized version of the N -body potential by averaging the direct-summation forces at 4 azimuths spaced 90° apart. Figure 2 shows the rotation for both cases as well as the rotation curve of the two halos. We do find that the two disagree within ~ 8 kpc, but this is due to the fact that the SCF expansion relies on spherical harmonics as basis functions and it is therefore difficult to reproduce

³ <http://github.com/jobovy/galpy>

		M_{init} ($10^8 M_{\odot}$)	M_{now} ($10^8 M_{\odot}$)	R (kpc)	v_R (km/s)	v_T (km/s)	z (kpc)	v_z (km/s)	ϕ (rad)
Sgr Mass Models	Sgr	–	~ 1–4	16.7	227.2	65.8	-6.26	202.4	3.00
	Heavy	102	32	10.9	258.2	68.2	-4.28	187.9	2.95
	Medium	51	15	10.2	273.4	96.9	-8.99	162.0	2.87
	Light	10.2	10	13.6	248.8	76.6	-7.59	186.3	2.95
Velocity Models	Sgr	–	~ 1–4	13.8	217.5	34.1	-5.52	176.7	2.99
	Fastest	51	10	10.6	220.0	28.3	-5.64	136.8	3.00
	Sgr	–	~ 1–4	15.5	226.3	52.9	-5.96	191.2	2.99
	Fast	51	13	13.2	217.3	37.6	-5.17	165.7	3.01
MW Mass Models	Sgr	–	~ 1–4	17.8	225.8	78.8	-6.56	214.4	3.00
	Slow	51	18	15.5	224.2	63.5	-5.83	194.5	3.00
	Sgr	–	~ 1–4	19.8	231.2	100.6	-7.06	232.2	3.01
	Slowest	51	22	17.0	233.8	89.5	-6.69	215.8	2.98
MW Mass Models MWPI4-1 MWPI4-3	Sgr	–	~ 1–4	13.8	217.5	34.1	-5.52	176.7	2.99
	Fastest	51	16	13.5	217.9	33.5	-4.47	176.5	3.00
	Sgr	–	~ 1–4	16.8	222.2	66.9	-6.29	205.0	3.00
	Median	51	23	14.9	234.1	70.6	-5.92	198.83	2.98
	Sgr	–	~ 1–4	19.8	231.2	100.6	-7.06	232.2	3.01
	Slowest	51	40	19.7	225.6	97.9	-6.14	232.5	3.01
	Sgr	–	~ 1–4	13.7	221.1	33.2	-5.50	174.8	2.99
Fastest	51	9	13.4	218.8	32.5	-5.23	164.7	2.97	
MWPI4-3	Sgr	–	~ 1–4	16.9	220.3	68.1	-6.33	206.7	3.00
	Median	51	15	17.0	201.4	52.4	-5.32	186.7	3.02
	Sgr	–	~ 1–4	19.7	232.9	100.0	-7.04	231.2	3.00
Slowest	51	20	18.2	246.4	103.6	-7.46	223.6	2.98	

Table 2. Position of Sagittarius at $t = \text{now}$ compared to each of the simulations. There is variation in the true position of Sgr because we consider orbits drawn from the uncertainties in Sgr’s current position to obtain the different kinematics of Sgr.

a disc-like structure. In all of our simulations, Sgr does not come within 10 kpc of the centre of the Milky Way, so the halo will be the component that most affects the dynamical friction and orbit of Sgr. It is therefore sufficient that the SCF approximation of the halo matches that of the exact simulation particles for the halo. Though not pictured, we also check the density profile of each component compared to the axisymmetrized density calculated using SnapshotRZ and found that much like the rotation curve, the two were consistent outside ~ 8 kpc.

We also ran a quick 100 Million particle simulation such that we could calculate the approximate mass of Sgr as a function of time. Using this as a model for mass loss, we were better able to predict the strength of the dynamical friction throughout the orbit. For both the density function required to calculate dynamical friction and the orbiting potential, we used our SCF potential approximation. To calculate the dynamical friction we use the ChandrasekharDynamicalFrictionForce from galpy which calculates the Chandrasekhar dynamical friction on a satellite given the mass, half-mass radius, position, and velocity of the satellite in a specified background potential. We initialise the dynamical friction object using the half-mass radius and total mass of the combined dark matter and stellar component of each Sgr model. For the potential in which the satellite is moving we use the SCF potential calculated for the equilibrium initial condition. Next, as we integrate the satellite backwards, we update the mass of Sgr after each of 1000 equally spaced integrals in the total integration time using the results of the 100 Million particle simulation. This is only a rough estimate of mass loss for two reasons. First, the mass loss is going to change between simulations as the orbit and Milky Way density changes, so using the mass loss from our test simulation

won’t be exactly accurate. Second, we do not change the half mass radius for each interval which means the Sgr will be approximated as too diffuse. However, we find that despite these assumptions, our placement of Sgr results in a fairly accurate final position in our simulations.

In each section of our analysis, we have a more thorough discussion of how we choose the final position of Sgr in each simulation because it depends on the Milky Way potential, the Sgr model, and the Sgr orbital kinematics. Once we know where we want Sgr to end, we integrate the orbit back two apocentres. We do this for several reasons. First, we go back to an apocentre because the modeling assumption that the disc is in equilibrium before the interaction is best satisfied when Sgr is at an apocentre so it is perturbing the disc as little as possible to start. Second, we go back two apocentres because we want to go back far enough to get the secondary effects from the passage, but longer than two apocentres, and the perturbation from the first pericentre passage has already phase-mixed and is no longer visible in the distribution function as seen in BB21.

Once we have the position and velocity of Sgr’s orbit two apocentres ago, we use it to place our Sgr particles in our simulation and truncate all particles at 500 kpc because the N -body integrator cannot deal with the distances generated by GalIC, $\sim 10,000$ kpc. While we use this method to try and estimate where the satellite will end up later in the simulation, it does not guarantee it will finish where we expect.

2.6 Sgr properties throughout the simulation

Throughout the simulation, we track the Sagittarius particles to obtain the orbit and effective mass of the satellite. This is important if

we want to compare the asymmetry in the simulation to the model developed in BB21. To do this, we use `clustertools`⁴(Webb 2020), a `PYTHON` package developed to retrieve the properties of clusters in simulations. We start by initializing a cluster using the positions, velocities, and masses of both the stellar and dark matter particles in our satellite. We can then use `clustertools` to find the central density of our cluster, the mass within the tidal radius, and the half-mass radius.

When setting up our simulation, we did our best to place the satellite such that it would end up around Sgr’s current position. However, we could not predict its path exactly, so once the simulation had finished, we chose the snapshot which most closely resembled the location and velocity of Sgr. Table 2 shows the current position of Sgr alongside the closest position of our satellite in the different simulation scenarios. For the three different Sgr mass simulations, the benchmark position does not change. However, by definition, when we look at how the uncertainty in Sgr’s current day position affects the orbit and therefore the perturbation, the benchmark changes. In some cases, we see the mass increase from one time step to another. This is because we define the mass as the total mass from Sgr particles within the tidal radius of the progenitor. Since Sgr has just passed through pericentre, some of the stream particles catch up to Sgr from one time-step to another therefore artificially increasing the observed mass of Sgr.

3 INVESTIGATING THE SOLAR NEIGHBOURHOOD

In this section, we investigate how both the mass of Sgr and its kinematic properties affects the asymmetry and mean vertical velocity in the solar neighbourhood. The density, which is used to calculate the asymmetry, and the mean vertical velocity are the zeroth and first velocity moment of disturbed phase-space spirals. For this reason, we will also look at the phase-space spiral.

Before placing Sgr, the solar neighbourhood could exist at any ϕ value in the simulation. However, by placing Sgr, the symmetry is broken and the solar neighbourhood is now at $R = 8.1$ kpc and $\phi = 0$ when $t = \text{now}$. Table 2 shows the final positions of Sgr in our simulations alongside the true position of Sgr in the Milky Way. For each simulation we find the two nearest snapshots because our orbits in the SCF potential are not able to exactly predict the orbit and therefore none of the snapshots are exactly correct. Once we have the closest snapshots, we choose the snapshot which has the closest z position and v_z velocity to the true Sgr position using the following equation:

$$\Delta = \sqrt{\left(\frac{z_{\text{sim}} - z_{\text{true}}}{8 \text{ kpc}}\right)^2 + \left(\frac{v_{z,\text{sim}} - v_{z,\text{true}}}{220 \text{ km s}^{-1}}\right)^2} \quad (5)$$

where the subscript ‘sim’ denotes the simulation’s position and velocity and ‘true’ denotes the position where we placed Sgr when integrating backwards. We also looked at the asymmetry and mean vertical velocity for both snapshots and found that they were very similar considering the uncertainties, and therefore it was not worth plotting both.

To select the solar neighbourhood, we adjust for the centre of mass and angular momentum of the disc, such that the disc is centered on our coordinates and is aligned with the plane $z=0$. This allows us to choose the location similar to the solar neighbourhood in distance from the centre of the disc. Once we have done that,

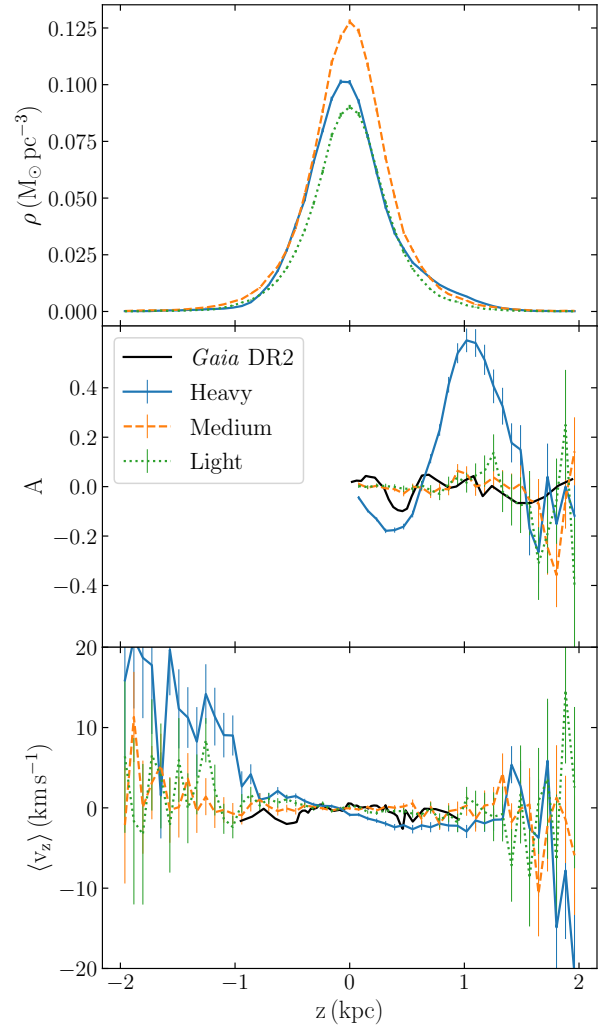


Figure 3. *Top:* Vertical density of solar neighbourhood-like sections of the simulation in cylinders with a radius of 250 pc at $R = 8.1$ kpc and $\phi = 0$ for three different Sgr mass models. From heaviest to lightest Sgr mass model, the Sgr models in each simulation are Heavy (blue solid), Medium (orange dashed), and Light (green dotted). *Middle:* Vertical number count asymmetry for the same volumes and simulation as the top panel. Only $z > 0$ is plotted as the asymmetry is anti-symmetric by definition. The black line shows the Gaia asymmetry from Bennett & Bovy (2019). *Bottom:* Mean vertical velocity for the same volumes and simulations. The mid-plane densities are all near the true value of the Milky Way mid-plane density ($0.1 M_{\odot} \text{pc}^{-3}$). None of the asymmetries are consistent with the Gaia data in shape or in amplitude. The mean vertical velocities do not achieve any true signal within the range of the data to determine a definitive match or mismatch.

we use a distance cut on the stars’ coordinates to select a cylinder with a radius of our choosing times 2 and re-calculate the angular momentum to remove any tilt from the warp of the disc. This ensures that the particles we extract from the simulation are getting a sun-like view and are therefore comparable to the data from Gaia DR2.

3.1 Changing Sgr mass

We start by looking at the effect of changing Sgr’s mass on the vertical perturbations to the disc. While this might seem like a simple scaling problem at first, changing Sgr’s mass will also affect

⁴ <https://github.com/webbj/clustertools>

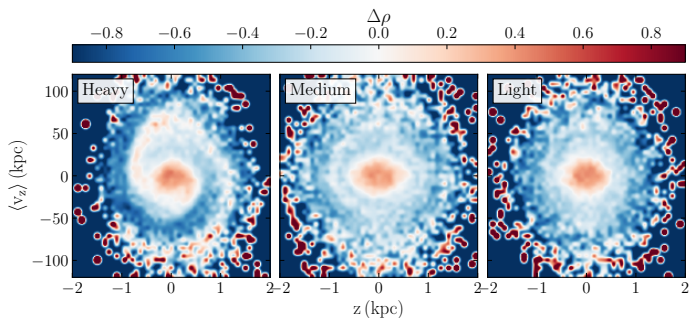


Figure 4. Phase space density for three simulations with varying Sgr mass models from heaviest on the left to lightest on the right. The volume considered is a cylinder centered at $R = 8.1$ kpc with a radius of $r_{cyl} = 250$ pc. The phase space spiral is clearly seen in the heavy simulation, but is faint in both the Medium and Light model. None match the phase-space spiral found in *Gaia* DR2 in both the amplitude and the tightness of the spiral.

the dynamical friction and therefore the orbit of Sgr, complicating matters. In our simulations, we choose Sgr mass models: Sgr1, Sgr2, and Sgr3 from BB21 as described in Section 2.2, referred to as Heavy, Medium, and Light models respectively throughout the rest of the paper. These satellites orbit in MWP14-2 from BB21 as described in Section 2.1. We do not investigate the other two models discussed in BB21, Sgr4 and Sgr5, as the amplitude from Sgr3 is already too small to match the observed perturbation, so a smaller Sgr model certainly would not reproduce the perturbation either.

The middle panel of Figure 3 shows the asymmetry for each of the Sgr models in our simulation at the solar neighbourhood. In BB21, we found that decreasing the mass of Sgr decreased the amplitude of the asymmetry and increased the period. It is clear that from the Heavy model to the Medium model, the amplitude of the asymmetry decreases drastically. Due to the size of the uncertainties, it is difficult to tell how the amplitude changes between the Medium and Light models, but if we zoom in on $|z| < 1$ kpc where the uncertainties are smallest, we find that the amplitude of the asymmetry in the Medium model is larger than the amplitude in the Lightest Sgr simulation as expected. In terms of the period of the oscillation, we see that the wavelength of the asymmetry decreases from the Heavy to the Medium model, but then increases from the Medium model to the Light model. This is inconsistent with our model. The model developed in BB21 assumed the perturbation was small so we would not expect it to be accurate for the Heavy simulation. In the case where the perturbation is small, we do see that the asymmetry wavelength increases from the Medium to the Light model. Finally, the black lines in Figure 3 shows the measured asymmetry from *Gaia* DR2 taken from Bennett & Bovy (2019). Clearly, none of the simulations are a match for the asymmetry. This is not surprising given that the only model that was even close to matching the data in Bennett & Bovy (2021) was the fastest moving model, and these are all the median speed models.

The last panel in Figure 3 shows the mean vertical velocity as a function of height in the three different simulations. The Heavy model can immediately be ruled out as a match given the very evident breathing mode near the mid-plane which is not seen in the data. Unfortunately, the data only goes out to 1 kpc and at those distance, the amplitude and uncertainties in the mean vertical velocity in the Medium model and the Light model means we cannot determine whether they are a match or not.

The asymmetry and mean vertical velocity are both derived

from the phase-space density. Figure 4 shows the phase-space spiral for the three simulations. In the left panel, we see a one armed spiral similar to that seen in *Gaia* DR2 from the heaviest model. However, the amplitude is too large by more than a factor of 2 and the spiral is much too loosely wound. By 1 kpc, the spiral in *Gaia* DR2 has wound around twice, whereas our simulation has only wound once. For both the Medium and Light model, we can see a very faint spiral, but as seen in the asymmetry, the perturbation is very small within $|z| < 1$ kpc. The amplitude is clearly not what we see in the *Gaia* data, but it is difficult to tell how the period of the spiral compares to the data given the weak signal. Other works with well resolved spirals typically have Sgr mass models on the order of our Heavy Sgr (Laporte et al. 2019; Hunt et al. 2021), therefore the faint spiral in our Medium and Light Sgr model is not unexpected.

After looking at how changing mass affects the perturbation to the solar neighbourhood, it is safe to conclude that the median velocity orbit for any of the models will not result in a match to the *Gaia* DR2 data. Our next step is to investigate whether or not changing the kinematics of Sgr will help achieve a match.

3.2 Changing Sgr kinematics

Due to the uncertainty in the position and velocity of Sgr, there is some wiggle room in its orbit. Another parameter that can significantly affect the shape of the asymmetry is the speed at which Sgr was travelling when it passed through the mid-plane of the disc, $v_{z,through}$, and how long ago that occurred, $t_{through}$. These two parameters are highly correlated for the current uncertainties in its present phase-space position and in the Galactic potential, so looking at different velocities of Sgr corresponds to also looking at different times since passing through the disc. For our investigation of the kinematics of Sgr, we chose to use the Medium model since the asymmetry from the Heavy simulation had a very large amplitude and the amplitude from the Light model was very small and not consistently above the uncertainty in the points. It is worth noting that in our investigation into the effects of the mass of Sgr, even the lightest model finished with a mass which was too large compared to the observed mass of the Sgr progenitor today. We are choose to use the Medium model, because it is the most likely to reproduce the amplitude of the perturbation. Furthermore, if we find that the amplitudes of the asymmetry are still not large enough, we are able to rule out the Light Sgr model as seen in Section 3.1.

In BB21, we investigated Sgr’s orbit as a function of the uncertainties in its current position. We sampled 10010 initial conditions from the uncertainty distributions in the current positions and velocities of Sgr (Gaia Collaboration et al. 2018c). Using these orbits, we calculated the velocity through the mid-plane and the time since passing through the mid-plane for each. For the purpose of this paper, we bin the orbits by their velocity through the mid-plane into nine bins and run simulations for the first (fastest), third (fast), fifth (median), seventh (slow), and ninth (slowest) bin. This allows us to cover a the entire range of Sgr velocities with our simulations.

Figure 5 shows the vertical density distribution, vertical number count asymmetry and mean vertical velocity for our four different Sgr velocity simulations. In BB21, we found that changing the mid-plane density did not affect the shape of the asymmetry, but increased the amplitude as well as the perturbation wavelength. It had the same effect on the mean vertical velocity, changing the mean vertical velocity and asymmetry but not the shape. This will be important when looking at the asymmetry and mean vertical velocity in our simulations.

The second panel of Figure 5 shows the asymmetry for the

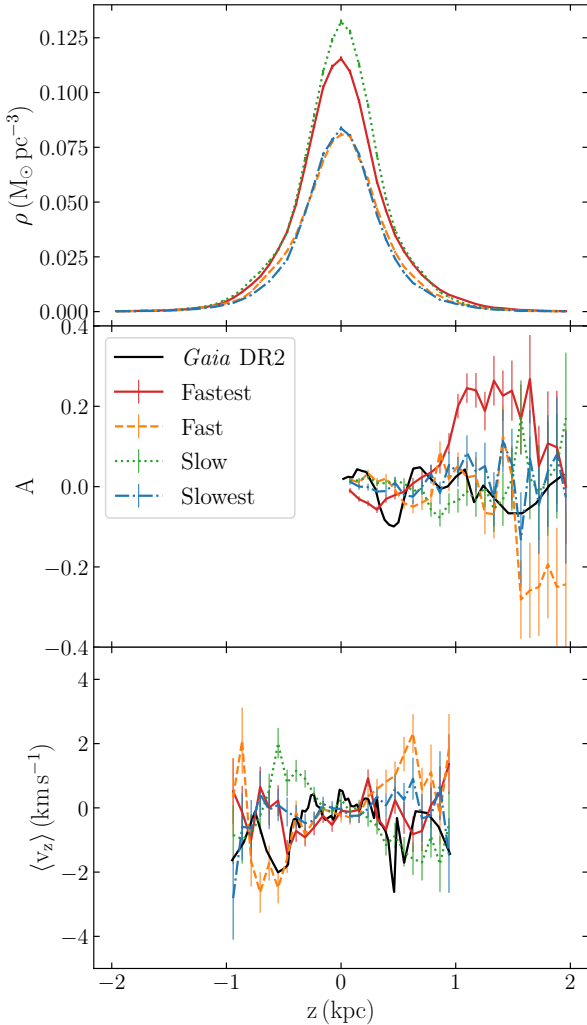


Figure 5. *Top:* Stellar density as a function of height in a solar neighbourhood-like location. The volume considered is vertical cylinder with a radius of 250 pc at a position of $R = 8.1$ kpc and $\phi = 0$. The four coloured line indicate the four different Sgr orbit models: Fastest (red solid), fast (orange dash), slow (green dot) and slowest (blue dash-dot). *Middle:* Vertical number count asymmetry for four different Sgr velocity simulations. Only $z > 0$ is plotted as the asymmetry is anti-symmetric by definition. The black line shows the *Gaia* asymmetry from Bennett & Bovy (2019). *Bottom:* Mean vertical velocity in the solar-neighbourhood-like volume. The uncertainties in the simulation outside $|z| < 1$ were larger than the signal. Since we only have the *Gaia* data within the same heights, we choose to omit the simulation values outside that area as well. The mid-plane densities vary between $(0.08 - 0.13) M_{\odot} \text{pc}^{-3}$, which spans the true value of the Milky Way mid-plane density. None of the asymmetries or the mean vertical velocities match the *Gaia* DR2 observations.

four different velocity simulations. None are a good match for the observed *Gaia* DR2 asymmetry. Our model in BB21 showed that as the $v_{z,\text{through}}$ increases, the asymmetry wavelength decreases. The amplitude of the asymmetry does not show a clear trend as the velocity of Sgr decreases or increases. This is because the change in amplitude doesn't come from a linear change like the mass of Sgr, but from a change in the orbit which brings it either closer or further away from the solar neighbourhood. We can see from our simulations that the asymmetry wavelength does decrease as we increase the speed of Sgr. None of the simulation asymmetries are

a match for the data, the closest is the 'Fast' simulation which is the nearest in shape, but has the wrong amplitude and asymmetry wavelength. It is worth noting that the mid-plane density of the Fast model is smaller than the true mid-plane density of the disc. Since it appears that the Fast simulation follows the trends seen in the model, we can discuss how we would expect the asymmetry to change by increasing the mid-plane density. Though it might increase the amplitude slightly, increasing the mid-plane density would also increase the asymmetry wavelength, making the asymmetry in the simulation even further from the true observed asymmetry.

It is also important to consider how the mean vertical velocity in the asymmetry compares with the true signal in *Gaia* DR2. In the data, BB21 found a bending mode in the solar neighbourhood within $|z| < 1$. This was later confirmed by Carrillo et al. (2019) who found a bending mode within $|z| < 1$ and a breathing mode further out. Both the Fast and Slow simulation show breathing modes which is inconsistent with the data. This means that even though the Fast simulation was the best match for the asymmetry, although still a pitiable match, the signal in the mean vertical velocity is drastically different than what is observed. The Slowest simulation has no notable breathing or bending signal as it is consistently within the uncertainty of zero. The Fastest simulation is the only one with a bending signal, but the amplitude is far off from the true amplitude from *Gaia* and the asymmetry associated with the Fastest simulation is the furthest from the observed asymmetry.

We can therefore conclude that changing the velocity of Sgr is not enough to make the simulated perturbation match the observed perturbation. This is even more obvious when we note that the simulations used in this Section are run using the Medium Sgr mass model. In Section 3.1, we established that the Medium mass model was still too large in terms of the progenitor mass. So not only is the perturbation not a match for any of the simulations, but the second heaviest Sgr model is not enough to create the observed amplitude in the asymmetry and it is even still too large.

3.3 Changing Milky Way Halo Mass

Our final investigation looks at how changing the mass of the Milky Way changes the perturbation in the simulation. To do this, we use the medium Sgr mass model (Sgr 2). Though we have found that the final mass of the medium Sgr is consistently too large, we want to ensure that the signal is large enough to see in our simulations. We also look at the fastest, median, and slowest Sgr velocities for each of the Milky Way models. Again, we bin orbits by their velocity through the mid-plane ($v_{z,\text{through}}$) for each of the Milky Way models. The fastest, median, and slowest Sgr orbits correspond to the first, fifth, and ninth bin (out of nine bins). One other consideration in this section is that the slowest Sgr orbit in MWP14-1 is only integrated back one apocentre before being placed. This is because the second last pericentre occurred ~ 8 Gyr ago and all effects from that apocentre would have phase mixed, so in that case only, the shape of the perturbation is set only by the most recent pericentre passage.

In BB21 we found that the mass of the Milky Way had a significant effect on the shape and amplitude of the perturbation, especially the asymmetry. Because we want to look at the various velocities in two more Milky Way models, which each require new initial conditions to be set up and run to equilibrium, we decided to halve the number of particles, therefore all simulations in this section have approximately 500 million particles and the initial conditions are initialised using GaLIC as described in Section 2.1 using the values from Table 1. We choose to run simulations with

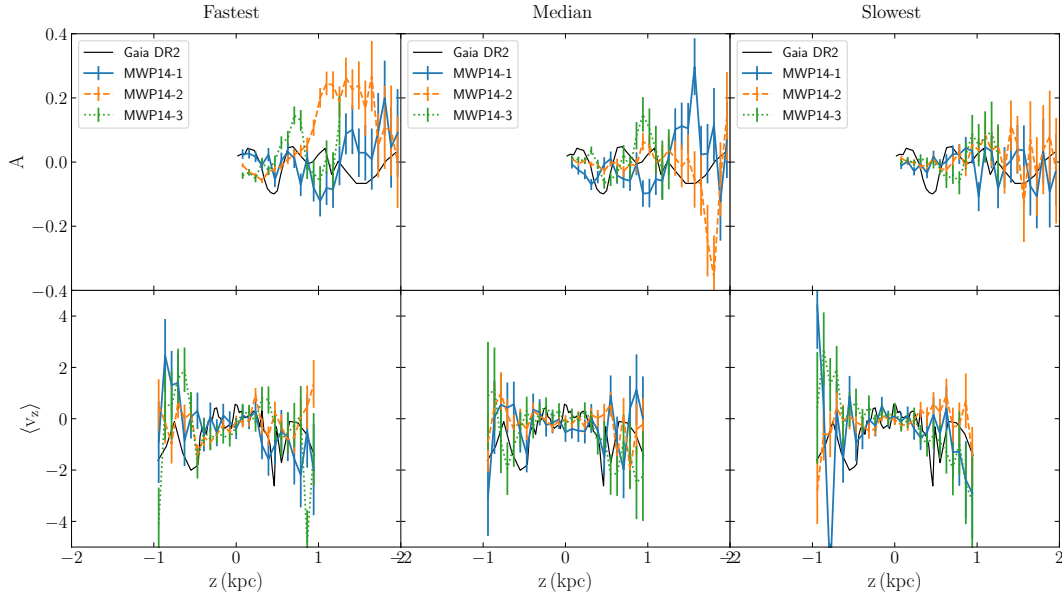


Figure 6. *Top:* Number count asymmetry of the three different Milky Way halo simulations for three different kinematics of Sgr from Fastest on the left to Slowest on the right. The three different Milky Way halos include the lightest MWP14-1 (blue solid), the medium halo MWP14-2 (orange dashed), and the heaviest halo MWP14-3 (green dotted). For MWP14-3, we have only plotted the asymmetry out to $z = 1.3$ because the uncertainties become quite large further out and obscure the shape of the asymmetries. *Bottom:* Mean vertical velocity for each grouping of Sgr kinematics and Milky Way halo mass. To match the data, we limit the calculations to $|z| < 1$ kpc. For both, the observed *Gaia* DR2 observations are plotted in black. The closest match to observations is the median Sgr orbit for MWP14-3, though it is still far from a perfect match.

all three Milky Way mass halos to cover the full span of possible masses, though we expect MWP14-2 or MWP14-3 to provide the best match based on the results of BB21. For MWP14-3, we found that the outer reaches of the disc took longer to reach equilibrium in our isolated Milky Way simulation, so the equilibrium simulation was run for 5 Gyr instead of 3 Gyr.

In Figure 6, we show the asymmetry and mean vertical velocity for the three different Milky Way models. The three different panels are the fastest, median, and slowest Sgr orbit from left to right. In BB21, we found that as we increased the Milky Way halo mass in general, the asymmetry wavelength and the asymmetry amplitude increased. This was not consistent across all Sgr models and all Sgr kinematics, but held in most cases. These trends are visible to some extent in Figure 6 especially in the slowest panel. We see that for the slowest Sgr orbit, the amplitude of the asymmetry increases as we increase the mass of the halo as does the perturbation wavelength. In the fastest panel, the shape of the asymmetry is fairly different between the three different halo models. However, things are more complicated in the median panel. When comparing MWP14-2 and MWP14-3, we see an increase in the amplitude as we increase the mass of the halo. However, we see that MWP14-1 actually has a fairly large amplitude for the fastest and median Sgr orbit simulation. This is likely because the mid-plane density in those two MWP14-1 simulations is much smaller (approximately $2\times$ smaller) than the mid-plane density for the other two simulations. However, the mid-plane density in the slowest Sgr orbit simulation matches the mid-plane densities seen in MWP14-2 and MWP14-3, which is why the trend in the amplitude holds there. This likely happens because the disc in the MWP14-1 gets more fluffed up by the fastest and median Sgr than the disc in the other simulations, likely due to the smaller restoring force from the lighter halo and a faster moving Sgr. In the slowest velocity MWP14-1 simulation, the speed of Sgr is small enough that it doesn't heat the disc as much. From the trends seen in

BB21 as well as the slowest simulation, we can therefore conclude that the discrepancies seen in the median MWP14-1 simulation is solely due to the small mid-plane density and would likely follow the same trends if we increased the mid-plane density. In BB21, we saw that increasing the mid-plane density decreases the amplitude of the asymmetry and decreases the asymmetry wavelength which would make the simulations from MWP14-1 even further from a match to the observations. The uncertainty in the mean vertical velocity is too large for all three simulations to uncover any true trends from one Milky Way model to the other.

In BB21, we found that MWP14-3 resulted in the perturbations with the most accurate shape, but consistently found that the asymmetry wavelength was too large. In our simulations, the model with the asymmetry and mean vertical velocity most similar to the *Gaia* DR2 observations is the median velocity Sgr in MWP14-3, the heaviest halo. The asymmetry for that simulation is the best match for the dip in the asymmetry at $z \approx 0.4$ kpc, but it still far from an exact match. The dip in the asymmetry of the simulation is centred closer to $z = 0.6$ kpc. Furthermore, the peak in the simulation asymmetry at $z \approx 0.9$ is not seen in the *Gaia* DR2 data. If we look at the mean vertical velocity for the same simulation it appears there might be troughs at $z = \pm 0.8$ kpc. However, it is difficult to tell for sure with the uncertainties. If we calculate the breathing and bending mode amplitudes however, we find that the amplitudes of both are within uncertainty of each other. Meaning the symmetric vs. anti-symmetric components of the velocity are approximately equal. In Figure C.6 of Gaia Collaboration et al. (2018b) we see that there should not be any amplitude of a breathing mode at the Sun's location out to 1.2 kpc, let alone a breathing mode with approximately the same amplitude as the bending mode. Furthermore, the final mass of Sgr in that simulation is approximately $15 \times 10^8 M_{\odot}$, which is approximately 4-15 times too large compared to the measured mass of the Sgr progenitor (Vasiliev & Belokurov 2020)

and yet the amplitude of the dip in the asymmetry near $z = 0.5$ kpc is still too small. Therefore, while we can conclude that the median Sgr velocity model for MWP14-3 is the best at reproducing one feature of the asymmetry, it is not a good match.

4 DISCUSSION & CONCLUSION

In this paper, we described a thorough method for initializing Milky Way initial conditions derived from the properties of `MWPotential2014` in `galpy`. Table 1 gives the full list of `GalIC` parameters for each of the three equilibrium galaxies in our simulations. For computational reasons, we ran the `GalIC` initial conditions for 1/10th of the particles ten times using different random seeds. We underwent a similar (though much more simple) method for generating the initial conditions for three different Sgr mass models. Once we had the initial conditions, we evolved each galaxy for 3+ Gyr in isolation. We did this to ensure that the solar neighbourhood was in fact in equilibrium. In all three galaxies, a bar formed in the centre of the galaxy, much like it did in the Milky Way. We then looked at the properties of the final snapshot of the equilibrium galaxies, including the asymmetry at eight different solar neighbourhood-like volumes around the simulated Milky Ways.

Once we had the initial condition, we had to figure out where to place the Sgr particles such that they would finish near the true Sgr position. This is fairly complicated as it involves estimating the Milky Way potential, mass loss of Sgr, and dynamical friction. We solved the first dilemma by calculating an SCF potential expansion of the N -body particles to estimate the true potential of the unperturbed simulation. To take into account the changing mass of Sgr in the calculation of dynamical friction, we estimated the mass loss of Sgr by running a 100 Million particle simulation of Sgr and tracking the virial mass throughout the simulation. This allowed us to estimate where to place Sgr in our simulations. Table 2 shows the final position of Sgr in all of our simulations as well as the 'True' position.

In our simulations, we investigated three different properties of the simulation to see how it affected the perturbation to the solar neighbourhood. The first was the mass of Sgr. We found that the perturbation from the heaviest Sgr was much larger than both the observed asymmetry and the mean vertical velocity. Furthermore, it resulted in a strong breathing mode within $|z| < 1$ kpc, which is not observed in the Milky Way. Between the medium and the light Sgr, we found the medium Sgr had a slightly larger perturbation amplitude as expected, and a slightly shorter asymmetry wavelength.

Next, we looked at the effect of the uncertainty in Sgr's current day position on the observed perturbation. With such a large uncertainty in Sgr's current position, there is also a large uncertainty in its orbit. We characterise an orbit by the speed at which it passed through the disc most recently, $v_{z,\text{through}}$. We chose to look at four different orbits: Fastest, Fast, Slow, and Slowest. For these simulations, we chose to use the medium mass model of Sgr. Clearly the heaviest Sgr had resulted in a perturbation which was much too large. By looking at the second heaviest, which already had a very small asymmetry within $|z| < 1$ kpc, we could rule out lighter mass models if even the medium one failed to produce the perturbation amplitudes required to match the observed perturbation. We found that our considerations had been correct and none of the simulations were able to reproduce an asymmetry or mean vertical velocity similar to that observed in *Gaia* DR2. The most similar in shape was the Fast simulation, but its amplitude was too small and the asymmetry wavelength was too long. Furthermore, it

produced a breathing mode in the mean vertical velocity, which is not seen in the data.

Finally, we looked at how the Milky Way halo mass affects the observed asymmetry. While the sections on Sgr mass and Sgr kinematics used the medium mass halo for the simulations, we also looked at a light and a heavy halo. In the light halo simulation, we found that none of the perturbations were even similar to the observations from *Gaia* DR2. Furthermore, the small mid-plane density in the simulation also meant that the both the amplitude and wavelength of the asymmetry was over-estimated compared to the effect it would have on the Milky Way disc, making the match even worse. The heavy Milky Way halo simulation resulted in the best match of all the simulations considered. The simulation where Sgr was initialized with the median $v_{z,\text{through}}$ resulted in a dip in the asymmetry at approximately $z = 0.6$ kpc. However, the asymmetry for that simulation also contained a peak at $z = 0.9$ kpc which is not seen in the data. Furthermore, the mean vertical velocity contains a measurable breathing mode within $z < 1$ kpc which does not exist in the *Gaia* DR2 data. We therefore conclude that none of the simulations are able to reproduce the observed perturbation to the solar neighbourhood. Furthermore, in BB21 we found that including the Large Magellanic Clouds (LMC) in our calculations only increased the asymmetry wavelength and decreased the amplitude of the perturbation. Most of the trends seen in the model of BB21 have been confirmed here, so it is safe to assume that it would have the same effect on our simulation and would not resolve the discrepancy between our simulation and the *Gaia* DR2 observations.

Though our suite of simulations is more comprehensive than most preceding it, there are still limitations to our analysis. Thirteen simulations of the Milky Way and Sgr interaction is fairly numerous, but while we tried to cover the range of each parameter, our sampling within that range was fairly small. A further limitation of our analysis is that we are not able to control the mid-plane density of the solar neighbourhood. Which means we cannot force it to exactly match the mid-plane density of the Milky Way disc, something BB21 shows can affect the perturbation wavelength and amplitude. The lack of a gas disc is also a limitation of our simulations, though it is a fairly common simplification (Laporte et al. 2018; Hunt et al. 2021) and simply assumes that the gas approximately follows the stars. Finally, from our analysis in Section 3.3, we see that the mass of the halo, and therefore dynamical friction, has a large effect on the observed perturbation. Our simulations span halo masses of $(0.98 - 1.95) \times 10^{12} M_{\odot}$, which is a very large range to be covered by only three simulations. In our analysis, we were only able to look at three different Milky Way mass halos especially since they each had to be integrated for 3 or more Gyr each. While the span of the simulations is larger than has been considered before, there are still several areas of improvement.

Despite these limitations, we still feel fairly confident ruling out Sgr as the cause of the perturbations based on the results of our simulations. First, the final mass of Sgr in all of our simulations is significantly larger than the Sgr mass measured by Vasiliev & Belokurov (2020) as shown in Table 2. Despite them all having too large a mass, we still consistently find that the amplitudes within $|z| < 1$ kpc are too small with the exception of a couple of the Fastest models or the Heaviest Sgr, but none of which have the correct shape. Furthermore, the best measurements of the halo mass estimate it to be approximately 1.25×10^{12} (Deason et al. 2016; McMillan 2017). This would lie somewhere between MWP14-1 and MWP14-2, yet it was only the heaviest halo MWP14-3, which was able to reproduce a perturbations anything like the observed perturbation. That would

mean that the halo has to be approximately 1.5 times more massive than has been measured, a fairly large discrepancy. Even our best match from the simulations only had one feature which vaguely resembled the observed perturbations, but overall was a poor match. Much like our investigation in BB21, we conclude that Sgr could not have caused the perturbation of the solar neighbourhood on its own. We cannot rule out the possibility that Sgr might play some role in the perturbation, just that Sgr alone could not have caused them and other theories like a spiral+bar+Sgr coupling needs to be explored. Although the dependence of the perturbation on its mass combined with observational constraints on its mass mean that its contribution to the observed asymmetry must be small. It remains to be seen whether other proposed scenarios such as the buckling of the bar, or non-linear coupling between bar-buckling, spiral structure, and perturbations from satellites including Sgr can explain the vertical asymmetry in the solar neighbourhood.

ACKNOWLEDGEMENTS

MB and JB acknowledge financial support from NSERC (funding reference number RGPIN-2020-04712) and an Ontario Early Researcher Award (ER16-12-061). JASH is supported by a Flatiron Research Fellowship at the Flatiron institute, which is supported by the Simons Foundation. This work has made use of data from the European Space Agency (ESA) mission *Gaia* (<https://www.cosmos.esa.int/gaia>), processed by the *Gaia* Data Processing and Analysis Consortium (DPAC, <https://www.cosmos.esa.int/web/gaia/dpac/consortium>). Funding for the DPAC has been provided by national institutions, in particular the institutions participating in the *Gaia* Multilateral Agreement. A portion of the computations were performed on the Niagara supercomputer at the SciNet HPC Consortium (Loken et al. 2010; Ponce et al. 2019). SciNet is funded by: the Canada Foundation for Innovation; the Government of Ontario; Ontario Research Fund - Research Excellence; and the University of Toronto. This work was performed in part at Aspen Center for Physics, which is supported by National Science Foundation grant PHY-1607611. This work was partially supported by a grant from the Simons Foundation.

DATA AVAILABILITY STATEMENT

The data underlying this article are available in the article and in its online supplementary material.

REFERENCES

- Antoja T., et al., 2018, *Nature*, 561, 360
- Bédorf J., Gaburov E., Portegies Zwart S., 2012, *Bonsai: N-body GPU tree-code* (ascl:1212.001)
- Bennett M., Bovy J., 2019, *MNRAS*, 482, 1417
- Bennett M., Bovy J., 2021, *MNRAS*, 503, 376 (BB21)
- Carrillo I., et al., 2019, *MNRAS*, 490, 797–812
- Deason A. J., Mao Y.-Y., Wechsler R. H., 2016, *The Astrophysical Journal*, 821, 5
- Fux R., 1999, *A&A*, 345, 787
- Gaia Collaboration et al., 2018a, *A&A*, 616, A1
- Gaia Collaboration et al., 2018b, *A&A*, 616, A11
- Gaia Collaboration et al., 2018c, *A&A*, 616, A12
- Hernquist L., Ostriker J. P., 1992, *ApJ*, 386, 375
- Holmberg J., Flynn C., 2000, *MNRAS*, 313, 209
- Hunt J. A. S., Stelea I. A., Johnston K. V., Gandhi S. S., Laporte C. F. P., Bedorf J., 2021, arXiv e-prints, p. arXiv:2107.06294
- Ibata R. A., Lewis G. F., 1998, *ApJ*, 500, 575
- Jenkins A., et al., 1998, *ApJ*, 499, 20
- Jenkins A., Frenk C. S., White S. D. M., Colberg J. M., Cole S., Evrard A. E., Couchman H. M. P., Yoshida N., 2001, *MNRAS*, 321, 372
- Kawata D., Baba J., Ciucă I., Cropper M., Grand R. J. J., Hunt J. A. S., Seabroke G., 2018, *MNRAS*, 479, L108
- Khoperskov S., Di Matteo P., Gerhard O., Katz D., Haywood M., Combes F., Berczik P., Gomez A., 2019, *A&A*, 622, L6
- Kuijken K., Dubinski J., 1995, arXiv e-prints, pp astro-ph/9502051
- Laporte C. F. P., Johnston K. V., Gómez F. A., Garavito-Camargo N., Besla G., 2018, *MNRAS*, 481, 286
- Laporte C. F. P., Minchev I., Johnston K. V., Gómez F. A., 2019, *MNRAS*, 485, 3134
- Loken C., et al., 2010, in *Journal of Physics Conference Series*. p. 012026, doi:10.1088/1742-6596/256/1/012026
- Mackereth J. T., et al., 2019, *MNRAS*, 489, 176
- McMillan P. J., 2017, *MNRAS*, 465, 76
- Navarro J. F., Eke V. R., Frenk C. S., 1996, *MNRAS*, 283, L72
- Ponce M., et al., 2019, in *Proceedings of the Practice and Experience in Advanced Research Computing on Rise of the Machines (Learning). PEARC '19*. Association for Computing Machinery, New York, NY, USA, doi:10.1145/3332186.3332195, <https://doi.org/10.1145/3332186.3332195>
- Springel V., White S. D. M., 1999, *MNRAS*, 307, 162
- Tormen G., Bouchet F. R., White S. D. M., 1997, *MNRAS*, 286, 865
- Vasiliev E., Belokurov V., 2020, arXiv e-prints, p. arXiv:2006.02929
- Webb J. J., 2020, *webbj/clusterstools: clusterstools v1.0*, doi:10.5281/zenodo.4087227, <https://doi.org/10.5281/zenodo.4087227>
- Widmark A., Monari G., 2019, *MNRAS*, 482, 262
- Widrow L. M., Gardner S., Yanny B., Dodelson S., Chen H.-Y., 2012, *ApJ*, 750, L41
- Yanny B., Gardner S., 2013, *ApJ*, 777, 91
- Yurin D., Springel V., 2014, *GALIC: Galaxy initial conditions construction* (ascl:1408.008)

This paper has been typeset from a $\text{\TeX}/\text{\LaTeX}$ file prepared by the author.